Macromolecular Chemistry and Physics

Macromolecular Chemistry and Physics

RESEARCH ARTICLE

Morphology-Controlled Rheological and Non-Isothermal Crystallization Behaviors in Immiscible Polypropylene/High Density Polyethylene Blends

Ke Zhan[1] | Pixiang Wang[2] | Xueqi Wang[1] | Xiaomeng Li[3] | Shaoyang Liu[2] | Thomas Elder[4] | Brian Via[1] | Chuanbing Tang[3] | Yucheng Peng[1]

[1]College of Forestry, Wildlife and Environment, Auburn University, Auburn, Alabama, USA | [2]Center for Materials and Manufacturing Sciences, Departments of Chemistry and Physics, Troy University, Troy, Alabama, USA | [3]Department of Chemistry and Biochemistry, University of South Carolina, Columbia, South Carolina, USA | [4]Southern Research Station, USDA-Forest Service, Auburn, Alabama, USA

Correspondence: Yucheng Peng (yzp0027@auburn.edu)

Received: 9 April 2025 | **Revised:** 27 May 2025

Funding: This study was financially supported by the College of Forestry, Wildlife and Environment of Auburn University, the USDA National Institute of Food and Agriculture (McIntire Stennis project ALAZ00079), and the National Science Foundation (2132093).

Keywords: blends | crystallization kinetics | high-density polyethylene | polypropylene | rheological properties

ABSTRACT

Understanding the correlation between morphology and the fundamental behavior of blends is crucial for tailoring their properties. This study investigated the effects of phase morphology on mechanical performance, rheology, and non-isothermal crystallization kinetics of immiscible polypropylene (PP)/high-density polyethylene (HDPE) blends. Nanometer-scale HDPE phases dispersed within PP, co-continuous phases, and micrometer-scale PP phases dispersed within HDPE were formed at 75/25, 50/50, and 25/75 PP/HDPE weight ratios, respectively. Mechanical results indicated that the co-continuous morphology dissipated energy more efficiently than the matrix-dispersed morphology. Rheological results showed that nanometer-scale dispersion significantly enhanced the blend elastic modulus through the restriction effect at the interfaces. Non-isothermal crystallization kinetics were analyzed using Jeziorny-modified Avrami, Ozawa, Mo, and Kissinger models. Due to HDPE's heterogeneous nucleation effect, the crystallization temperature of PP was elevated, and the crystallization rate of the blend also increased with higher HDPE content. Furthermore, the blend with the 25/75 PP/HDPE exhibited a higher crystallization rate than neat HDPE, as the interfacial boundaries facilitated the alignment of HDPE chains. The higher crystallization activation energy calculated in the 75/25 PP/HDPE blend suggested that nanometer-scale dispersion imposed a more significant restriction on crystal growth compared to micrometer-scale dispersion.

1 | Introduction

Polyolefins are the most widely used commodity plastics, accounting for ≈57% of total global plastic consumption due to their outstanding mechanical properties, chemical resistance, easy processability, and inexpensive feedstocks [1–5]. Polypropylene (PP), high-density polyethylene (HDPE), and low-density polyethylene (LDPE) represent the majority of polymers within the polyolefin family [6, 7]. PP and HDPE are primarily utilized in the production of rigid packaging, while LDPE is favored for flexible packaging applications [8]. Annually, >220 million tons of polyolefin plastics are generated, and global recycling rates remain low with <1% for PP, ≈10% for HDPE, and 5% for LDPE [2, 9]. Most of these non-degradable polyolefins end up

accumulating in landfills or leak into the environment, resulting in serious plastic pollution [10–12]. Promoting the recycling of polyolefins is critical to addressing this environmental issue and fostering a sustainable future [13].

Post-consumer PP and HDPE are frequently commingled in the plastic waste stream due to their similar application scenarios and chemical structures [14]. Their similar densities make it challenging to separate PP and HDPE cost-effectively with current plastic recycling techniques, although they can be separated using sophisticated equipment at high costs [15–17]. Melt-reprocessing commingled PP and HDPE into a polymer blend is a promising strategy because it avoids the need for sorting and potentially results in a blend with multiple functionalities from both polymers [14, 18]. Thus, PP and HDPE have been extensively studied in the form of blends [19–29]. Notoriously, the immiscibility of PP and HDPE leads to phase separation during the melt-reprocessing and crystallization processes [29, 30]. This separation impacts the fundamental properties of the blend, typically resulting in poor mechanical performance [31]. Improving the performance of the PP/HDPE blend has been a difficult problem in the field of polymer science for several decades [25].

For a polymer blend, its mechanical properties depend not only on the properties of its individual components but also significantly on its behavior during processing. The rheological behavior of a polymer blend is critical for understanding its processability and mechanical properties. The viscoelastic property of the blend determines its response to applied stress, affecting its impact resistance, tensile strength, and elongation at break. Therefore, studying the rheological properties of PP/HDPE blends is essential for optimizing processing techniques and enhancing mechanical performance.

Souza et al. [32]. studied the rheological properties of PP/HDPE blends with HDPE as the dispersed phase. They observed that in the low-frequency region, the storage modulus of the blends exceeded that of neat PP and increased with higher HDPE content. The authors attributed this enhanced elasticity to the longer relaxation process of the dispersed HDPE phase. Meanwhile, with PP as the dispersed phase, the mechanical properties and rheological behaviors of PP/HDPE blends were investigated by Karaagac et al. [33]. They revealed that the addition of PP reduced both the complex viscosity and impact strength of the blends.

Currently, the research has shifted to how various compatibilizers and additives affect the rheological properties of PP/HDPE blends [34–37]. However, the effects of the morphologies of the matrix-dispersed phase and the co-continuous phase on the rheological behaviors of PP/HDPE blends have not been fully clarified and understood. More fundamental knowledge in this area is needed to optimize processing and develop effective performance modification strategies.

Moreover, crystallization kinetics are essential for predicting and controlling the microstructure and, consequently, the mechanical properties of polymer blends [38]. For binary semi-crystalline polymer blends, such as PP/HDPE, the crystallization behavior is particularly complex because each polymer has unique crystallization temperatures, rates, and structures. The interplay between these polymers during crystallization can cause one polymer to nucleate before the other, potentially acting as a nucleating agent or creating a physical barrier. Such interactions can significantly alter crystallite morphology, thereby profoundly influencing the mechanical properties of the blend. Zhou et al. [20]. proved that the crystalline structure and mechanical properties of PP/HDPE blends with HDPE as the dispersed phase are tailorable. This highlights the crucial need to thoroughly understand the crystallization behaviors of PP/HDPE blends with different phase morphologies and effectively control the crystallization processes to enhance their performance.

Jose et al. [39]. investigated the phase morphology and crystallization behaviors of PP/HDPE blends with different weight ratios. Their study revealed that phase morphology plays a critical role in influencing crystallization behavior. Notably, co-continuous morphology had a more pronounced effect on the degree of crystallinity than the matrix-dispersed morphology. Huang et al. [28]. found that the crystallization temperature and nucleation rate of PP decreased with increasing HDPE composition when HDPE was the dispersed phase. In the case of the co-continuous morphology, the presence of HDPE reduced the nucleation and growth of PP spherulites. When PP served as the dispersed phase, the crystallization process was notably retarded. Several other studies have also explored the crystallization behaviors of PP/HDPE blends [17, 27, 40].

However, most of these studies have concentrated on isothermal crystallization conditions. In contrast, thermoplastic production in actual industrial processes, such as foaming, extrusion, and injection molding, typically occurs under non-isothermal conditions with varying cooling rates [41, 42]. Chow et al. [42]. conducted non-isothermal crystallization kinetic analyses on a PP/HDPE blend; the influence of dispersed HDPE phases on the blend's crystallization rate and activation energy was slight in their work. Another investigation into the effect of HDPE addition on the non-isothermal crystallization behaviors of PP was conducted by Blom et al. [43]. They observed that adding low levels of HDPE reduced both the number and size of PP chains participating in forming ordered crystalline regions, consequently delaying the nucleation and subsequent crystallization of PP.

Further studies on the non-isothermal crystallization kinetics of PP/HDPE blends remain limited. Additionally, conflicting findings have been reported in this area. The addition of HDPE has been found to both accelerate and delay the crystallization process of PP in different studies [17, 43]. More detailed studies are needed to establish a correlation between the PP/HDPE blend's phase morphology and non-isothermal crystallization kinetics.

This study aims to understand how the PP/HDPE blend's phase morphology correlates with its rheological properties and non-isothermal crystallization kinetics, thus providing insights for relevant researchers and engineers to optimize the PP/HDPE blend's processing and tailor its mechanical properties. PP and HDPE were melt-compounded into blends with different weight ratios, and their morphology, mechanical properties, rheological behavior, and non-isothermal crystallization kinetics were characterized.

2 | Experimental Section

2.1 | Materials

Homopolymer PP 1024 and HDPE 8920 pellets were used in this study. The PP has a density of 0.900 g cm^{-3} and a melt index of 13 g/10 min at 230°C/2.16 kg, while the HDPE has a density of 0.954 g cm^{-3} and a melt index of 20 g/10 min at 190°C/2.16 kg. The molecular weight (MW) and MW distribution of PP and HDPE are shown in Figure S1. For PP, the number-average molecular weight (M_n), weight-average molecular weight (M_w), and polydispersity index (PDI) were 30 kDa, 206 kDa, and 6.85, respectively. For HDPE, the M_n, M_w, and PDI were 15.9 kDa, 105 kDa, and 6.63, respectively. All pellets were dried in a forced air oven (Model 52411-11, Cole-Parmer Inc., Vernon Hills, IL) overnight at 105°C to remove moisture before use.

2.2 | Preparation of PP/HDPE Blend

PP/HDPE blends were prepared in an internal mixer (Model 2128, C.W. Brabender Instruments, Inc., Hackensack, NJ, US), equipped with two counter-rotating roller blades. PP and HDPE pellets were manually dry-mixed in weight ratios of 75/25, 50/50, and 25/75 to simulate the commingled PP and HDPE found in real-life plastic waste streams. Subsequently, the PP/HDPE mixtures were gradually added into the mixing chamber for melt-compounding. The net chamber volume is 369 cm^3, and the mixer was operated in constant volume mode at a fixed rotor speed. Torque was recorded continuously throughout the mixing process, which was considered complete once the torque reached a steady value. The sample fed amount, temperature, time, and counter-rotating speed were 200 g, 200°C, 5 min, and 60 rpm, respectively. Afterward, the blends were scraped off the mixer while still in a molten state and allowed to solidify at room temperature. The resultant blends were ground into particles by a low-speed granulator (Model SG-2042NH, Shini Plastic Technologies, Inc., Willoughby, OH, US) loaded with a 3 mm sieve. The particles were dried in an oven overnight at 105°C to remove moisture prior to injection molding. A benchtop injection molding machine (Proto-Ject 150 HP, Manning Innovations, Inc., Halls, TN, US) was used to produce test specimens with customized aluminum molds. The specimens for mechanical testing were injection molded according to the corresponding ASTM standards, while the 1.5 mm thick sheets were produced using a specific mold for rheological measurements. The injection-molding temperature and pressure were 200°C and 51 MPa, respectively. Neat PP and HDPE were also subjected to the same melt-compounding and injection-molding processes for comparison purposes. All samples were stored in Ziploc bags to prevent moisture intrusion prior to characterization.

2.3 | Characterizations

2.3.1 | Mechanical Test

Mechanical properties of PP, HDPE, and their blends with different weight ratios were measured at 23 ± 2°C with a relative humidity of 50 ± 5%. Tensile testing was conducted according to ASTM D638 (Type IV) using a Mark-10 universal testing machine (Model F1505, Copiague, NY, US) with a load cell of 1000 N and a resolution of 0.5 N. An Epsilon extensometer (Model SN E109112, Jackson, WY, US) was used to determine the strain of the testing blends as the samples were stretched. The testing speed and initial strain rate were 5 mm min^{-1} and 0.1 min^{-1}, respectively. Average values of the tensile strength at yield, tensile modulus of elasticity (MOE), and tensile elongation at yield were calculated from five replicates and reported with their standard deviations as error bars. Flexural testing (three-point bending test) was carried out according to ASTM D790. A Mark-10 universal testing machine (Model ESM750S, Copiague, NY, US) with a load cell of 500 N and a resolution of 0.2 N was utilized. A support span length of 50 mm was employed, and the speed of crosshead motion was set at 1.34 mm/min for all samples. Five replicates were tested, and the average values were reported, including flexural strength at 5% strain and flexural MOE. Impact strength was evaluated according to ASTM D256 using an XJUD Digital Charpy Izod impact tester (Deli Group Co. Ltd., Ningbo, China). The average values and standard deviations of ten replicates were measured and reported. One-way analysis of variance (ANOVA) statistical analysis was conducted on the mechanical testing results using IBM SPSS software, with a significance level of $\alpha = 0.05$. Following the ANOVA analysis, Tukey's Honestly Significant Difference post-hoc test was applied to assess the effects of different levels within each factor group.

2.3.2 | Morphology

The fractured surfaces of PP, HDPE, and their blends, obtained from impact tests, were examined by scanning electron microscopy (SEM, EVO 50, Zeiss, Oberkochen, Germany) at an accelerating voltage of 20 kV. The fractured surfaces were sputter-coated with gold for 120 s in a sputter-coating device (Q150R, Electron Microscopy Sciences, Hatfield, PA, US). The diameters of PP and HDPE domains were measured using ImageJ software.

2.3.3 | Fourier Transform Infrared Spectroscopy

PP, HDPE, their blends were analyzed using Fourier-transform infrared spectroscopy (FTIR, Spotlight 400, PerkinElmer, Waltham, MA, US). An attenuated total reflection accessory with diamond/ZnSe crystals was employed. The transmittance was recorded from 650 to 4000 cm^{-1} with a resolution of 4 cm^{-1}. Sixty-four scans per spectrum were performed, and three replicates were determined for each sample.

2.3.4 | Rheological Measurements

Rheological properties of PP, HDPE, and their blends were investigated by a rheometer (HAAKE MARS 60, Thermo Fisher Scientific, Germany) equipped with a parallel plate geometry (diameter = 25 mm, gap = 1.3 mm). The circular specimens with a diameter of 22 mm and a thickness of 1.5 mm were prepared using a Gasket punch (General Tools, Cincinnati, OH, US). All rheological tests were conducted at 200°C. The linear viscoelastic region (LVR) was determined through amplitude strain sweeps

at a frequency of 10 rad/s (Figure S2). A strain of 2% was selected to ensure that all oscillatory tests remained well within the LVR. Oscillatory frequency sweeps were performed over an angular frequency (ω) range from 0.1 to 100 rad/s to measure viscoelastic properties. For the rheological creep-recovery test, a constant stress of 50 Pa was applied. The strain was recorded as a function of time during the first 300 s for the creep stage and during the subsequent 500 s for the recovery stage. All data were averaged over three replicates and presented with error bars to indicate standard deviation.

2.3.5 | Differential Scanning Calorimetry

Melting and crystallization behaviors of PP, HDPE, their blends were characterized through differential scanning calorimetry (DSC, Q20, TA Instruments, New Castle, DE, US). An amount of 7 to 9 mg of the samples was examined under a nitrogen atmosphere at a flow rate of 50 mL min^{-1}. Initially, the samples were heated from 40 to 200°C at a rate of 10°C min^{-1}, then held isothermally for 5 min to erase their thermal history. Subsequently, they were cooled to 40°C at cooling rates of 5, 10, and 15°C min^{-1} to gather crystallization data, and then reheated to 200°C at a rate of 10°C min^{-1} to observe melting behavior. The crystallization peak temperature (T_c) and enthalpy (ΔH_c) were determined from the cooling scan, whereas the melting peak temperature (T_m) and enthalpy (ΔH_m) were obtained from the second heating scan. At least two replicates were examined for each sample to ensure reproductivity. The degree of crystallinity (X_c) was calculated according to Equation (1): [44]

$$X_c\,(\%) = \frac{1}{wt.\%}\left[\frac{\Delta H_m}{\Delta H_{m0}}\right] \times 100 \tag{1}$$

where ΔH_m is the melting enthalpy of PP or HDPE; ΔH_{m0} is the melting enthalpy for a 100% crystalline sample of PP or HDPE; and *wt.%* represents the weight fraction of the individual PP or HDPE component in their blends. The ΔH_{m0} value for 100% crystalline PP was set as 205 J/g [45, 46], while the ΔH_{m0} value for 100% crystalline PE was assumed to be 290 J/g [47, 48]. The non-isothermal crystallization kinetics were investigated based on obtained crystallization data.

3 | Results and Discussion

3.1 | Morphologies

The fractured surfaces of neat PP and HDPE are shown in Figure 1. A smooth surface was observed for PP, indicating a typical brittle fracture characteristic. In contrast, the fractured surface of HDPE was relatively rough and featured a higher fracture surface area compared to PP, contributing to its higher impact strength as shown in Figure 4a.

The fractured surfaces of PP/HDPE blends are shown in Figure 2. At the 75/25 PP/HDPE weight ratio, the HDPE dispersed phases were uniformly distributed within the PP phase, with parts of them being stretched and pulled out by the applied force during impact testing. As shown in the high-magnification image in Figure 2b, the HDPE dispersed phases were finely distributed; however, the apparent gaps between the PP and HDPE phases were still observed, suggesting poor interfacial interactions. When the HDPE content in the blend increased to 50 wt.%, as shown in Figure 3c,d, a co-continuous morphology formed, with PP and HDPE phases interpenetrating each other, allowing both components to retain their individual characteristics. The interpenetrated structure enhanced mechanical performance primarily by reducing stress concentrations, where cracks typically initiate and propagate. This reduction in stress concentrations significantly lowered the possibilities of localized failure and ensured more uniform stress distribution across a larger area, thereby facilitating efficient energy dissipation. With the 25/75 PP/HDPE weight ratio, PP acted as the dispersed phase, distributed across the HDPE phase, resulting in an island-sea morphology. This is a typical morphology arising from the phase separation of immiscible binary polymer blends. PP droplets served as stress concentrators, weakening the stress transfer capacity of the HDPE network, and leading to reduced mechanical performance. A detailed mechanical analysis is presented in a later section.

The diameters of the HDPE domains in the 75/25 PP/HDPE blend and the PP domains in the 25/75 PP/HDPE blend were measured, and the results are shown in Figure 3. The majority of HDPE domains in the 75/25 PP/HDPE blend had diameters in the nanometer range (below 1 μm), with 65% of them falling between 200 and 600 nm. In contrast, only 6% of the PP domains in the 25/75 PP/HDPE blend were less than 1 μm, with most being in the micrometer range, with 57% of them measuring between 1 and 3 μm.

3.2 | Mechanical Properties

Mechanical properties of PP, HDPE, and their blends are shown in Figure 4. The impact strength, shown in Figure 4a, of the neat HDPE (3.70 kJ m^{-2}) was much higher than that of PP (1.49 kJ m^{-2}), reflecting the inherent toughness of HDPE. When the PP/HDPE weight ratio was 75/25, the impact strength of the blend (1.62 kJ m^{-2}) was statistically comparable to that of neat PP, despite the addition of the tougher HDPE phase. This is attributed to the poor interfacial interaction between the PP and HDPE phases, resulting from phase separation [49]. With the 50/50 PP/HDPE weight ratio, the impact strength of the blend was significantly improved to 2.90 kJ m^{-2}, attributed to the formation of a co-continuous structure [50], in which PP and HDPE interpenetrated throughout the blend. This interlocking structure created a complex pathway for energy dissipation, absorbing energy more efficiently than the sea-island structure [51]. The impact strength of the blend increased to 3.10 kJ m^{-2} when the HDPE content increased to 75 wt.%, because the HDPE became the dominant phase and absorbed the majority of the impact energy. However, it remained significantly lower than that of neat HDPE, due to phase separation between PP and HDPE that introduced weak points in the energy dissipation pathway.

The tensile strength at yield and tensile MOE are shown in Figure 4b and the corresponding stress-strain curves are provided in Supplied Figure S3. Both tensile strength and MOE of neat PP (30.9 MPa and 1.60 GPa) were significantly higher than those of neat HDPE (19.8 MPa and 1.00 GPa), stemming from

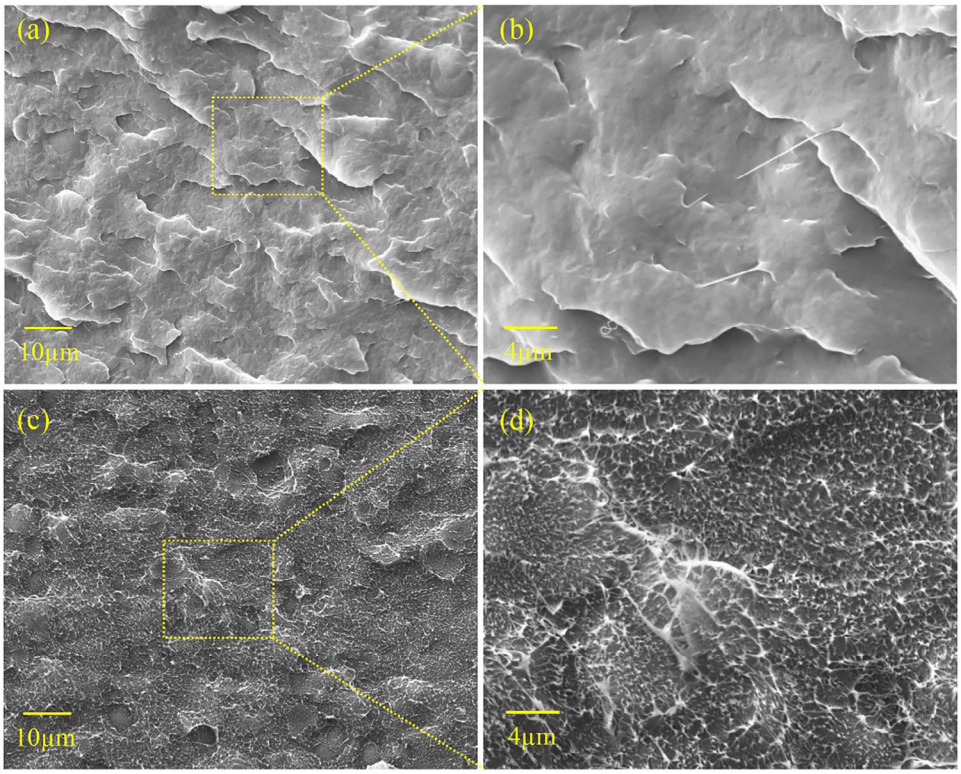

FIGURE 1 | Fractured surfaces of (a, b) neat PP and (c, d) neat HDPE.

PP's inherently greater strength and stiffness. As the PP content decreased, the blend exhibited a continuous decrease in both tensile strength and MOE. The tensile elongation at yield is shown in Figure 4c. Neat PP (8.22%) exhibited slightly lower elongation at yield compared to neat HDPE (8.99%), although the difference was not significant. The elongation of the blend with the 75/25 PP/HDPE weight ratio (7.72%) was slightly lower than that of neat PP, a result of incompatibility between the components. Similarly, the elongation at the 25/75 PP/HDPE weight ratio (8.68%) was also lower than that of neat HDPE for the same reason. However, the elongation at yield for the blend at the 50/50 weight ratio (8.82%) was comparable to that of neat HDPE, as the co-continuous structure at this ratio enhanced the interaction between PP and HDPE phases [52]. The flexural strength at 5% strain and flexural MOE are shown in Figure 4d. Similar to tensile results, both strength and MOE decreased with increasing HDPE content.

3.3 | FTIR Analysis

The FTIR spectra of PP, HDPE, and their blends are provided in Figure S4, and the corresponding band information for PP and HDPE is summarized in Table S1. All characteristic bands of individual PP and HDPE were found in their blends at the same positions, indicating that no chemical reaction occurred during the melt-compounding and injection-molding processes. The variations in mechanical properties, as well as the subsequent rheological and crystallization behaviors, were not attributed to any chemical changes.

3.4 | Rheological Properties

3.4.1 | Oscillatory Frequency Sweep

The frequency sweep results are plotted in Figure 5. As depicted in Figure 5a, the complex viscosity of PP was greater than that of HDPE across the entire testing frequency range of 0.1 to 100 rad/s. In the high frequency region (ω > 10 rad/s), obvious shear-thinning behaviors were observed for all PP, HDPE, and their blends. Polymer chains generally align in the flow direction under shear forces, reducing chain entanglements and consequently decreasing viscosity. This disentanglement was more pronounced at higher frequencies, as the polymer chains had less time to relax and return to their initially more entangled state [53]. At the 75/25 PP/HDPE weight ratio, the blend's viscosity remarkably increased compared to neat PP at angular frequencies below 0.4 rad/s. This enhanced viscosity can be attributed to the uniform dispersion of HDPE phases in nanometer scale within the PP matrix, as confirmed by the morphology in Figure 2b. The finely dispersed HDPE phases acted as effective barriers, restricting PP chain mobility, and thereby contributing to the observed increase in viscosity [54]. For the blends with 50/50 and 25/75 PP/HDPE weight ratios, similar trends of increased viscosity were observed as with the 75/25 ratio. These phenomena can also be attributed to the restriction effect between PP and HDPE phases due to immiscibility and viscosity difference.

The Cross model was employed to analyze polymer blends, the zero-shear viscosity (η_0) values of PP, HDPE, and their blends

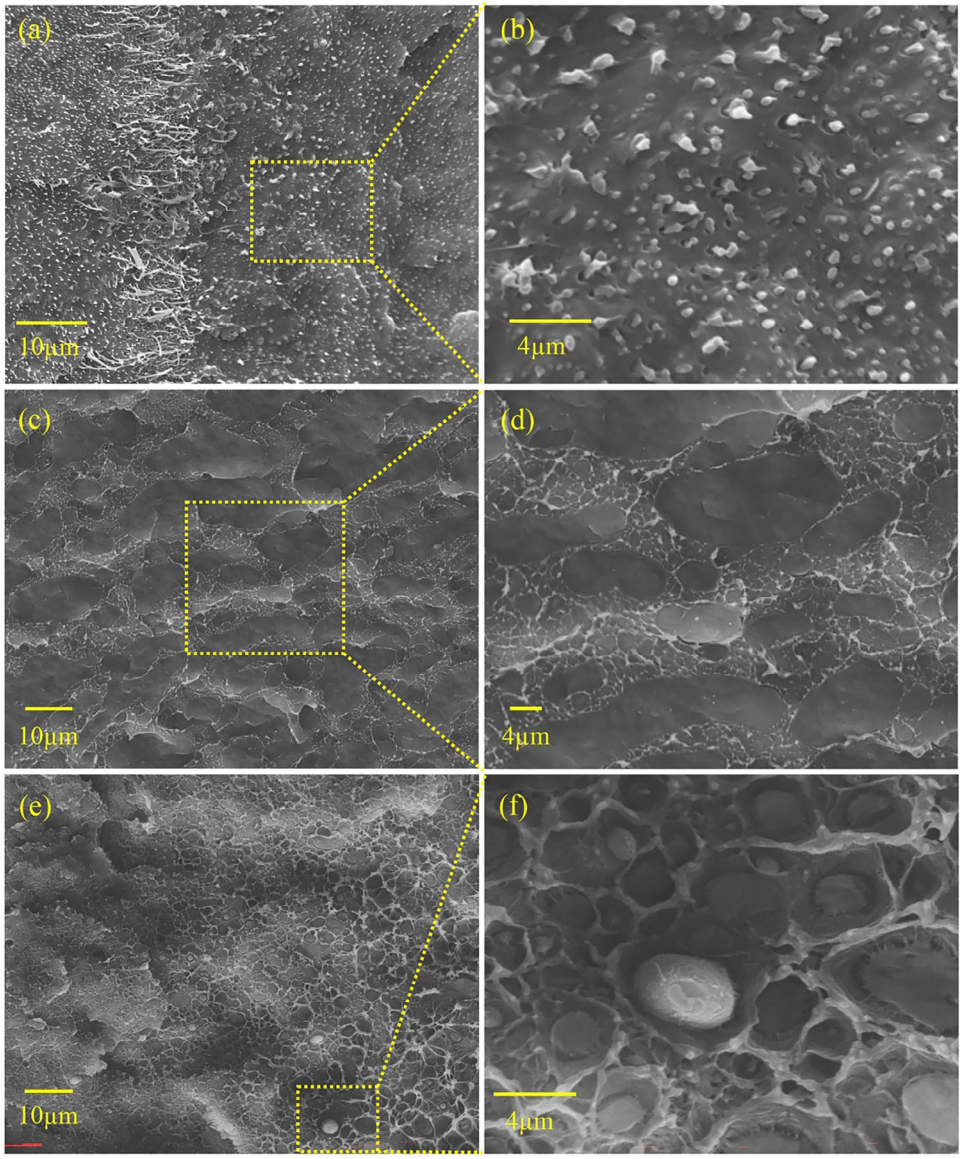

FIGURE 2 | Fractured surfaces of the blends with PP/HDPE weight ratios of (a, b) 75/25, (c, d) 50/50, and (e, f) 25/75.

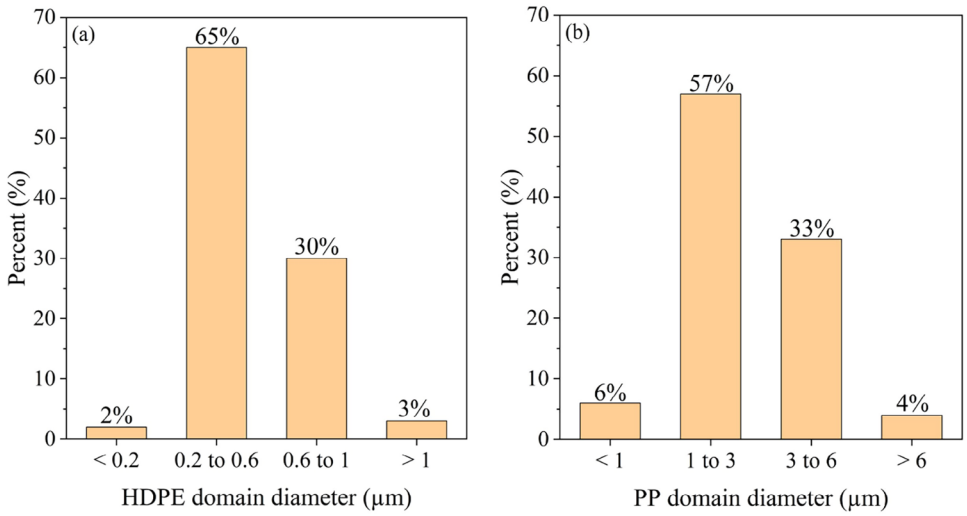

FIGURE 3 | Domain diameters of (a) HDPE in the 75/25 PP/HDPE blend and (b) PP in the 25/75 PP/HDPE blend.

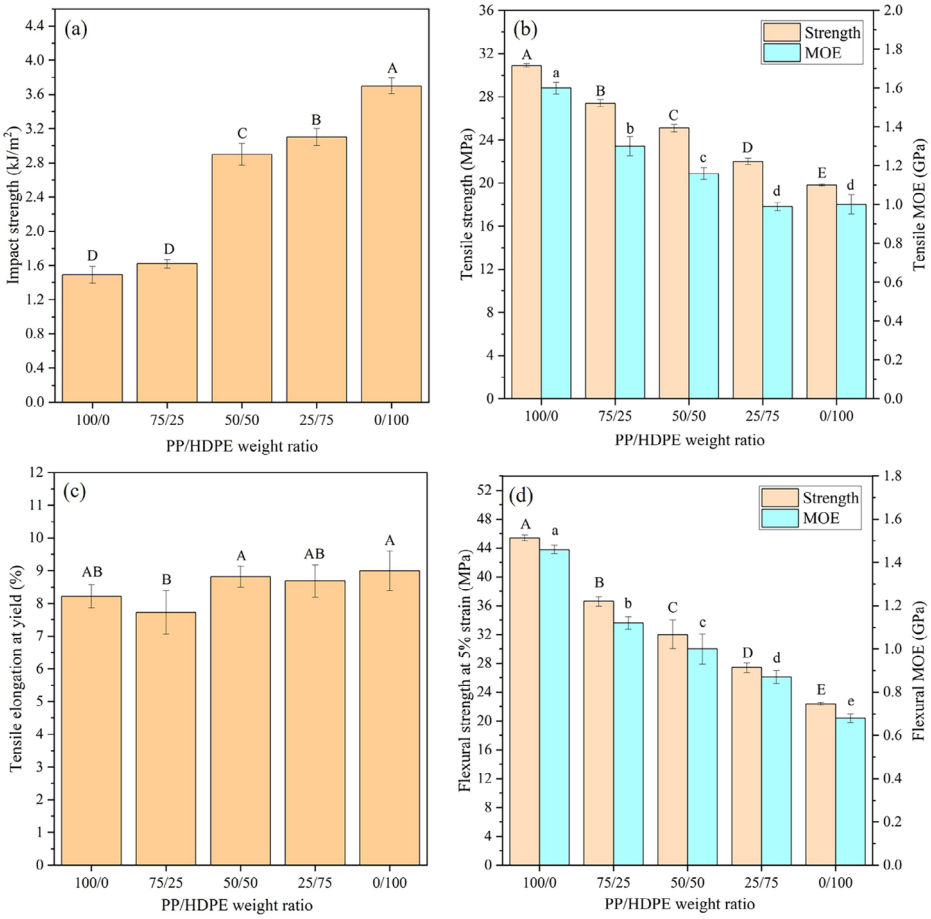

FIGURE 4 | Mechanical properties of PP, HDPE, and their blends (Both uppercase and lowercase letters represent the levels of statistical significance).

were fitted using this model [55, 56], as described by Equation (2):

$$\eta = \frac{\eta_0}{(1+\lambda\omega)^{1-n}} \quad (2)$$

where ω is the applied angular frequency, η is the measured complex viscosity, and η_0 is the fitted zero-shear viscosity. λ is the characteristic time in rheology, representing the timescale at which the material relaxes or returns to its original state after deformation. A higher λ value indicates a slower relaxation process. n is the power-law index, a dimensionless number that reflects the degree to which a fluid's viscosity changes with the shear rate, where $n < 1$ signifies shear-thinning behavior (viscosity decreases with increasing shear rate), $n = 1$ represents Newtonian behavior (viscosity remains constant regardless of shear rate), and $n > 1$ indicates shear-thickening behavior (viscosity increases with increasing shear rate). The fitted η_0, λ, and n values are shown in Table 1. The η_0 value of PP was 1439 Pa·s, distinctly higher than HDPE's 475 Pa·s, suggesting a greater MW for PP since the η_0 value generally correlates with MW [57]. For un-crosslinked polymers, this relationship typically follows the proportionality of $\eta_0 \approx MW^{3.4}$.

A much higher η_0 value of 2153 Pa·s was observed for the blend with the 75/25 PP/HDPE weight ratio, compared to neat PP, quantitatively demonstrating the impact of the nanometer-scale dispersion of HDPE phases within the PP matrix. The η_0 values for the 50/50 and 25/75 PP/HDPE blends did not show the same apparent changes as the 75/25 blend, likely due to size differences of the dispersed phases. In the 75/25 PP/HDPE weight ratio blend, the nanometer-scale dispersion of HDPE within the PP matrix significantly increased the interfacial boundaries between the PP and HDPE phases due to high contact area, leading to more pronounced restrictions on chain mobility. In contrast, in the blends with 50/50 and 25/75 PP/HDPE weight ratios, two phases existed in much larger sizes, as evidenced by SEM images in Figure 2, resulting in less restriction on polymer molecular movement.

The λ value of the neat PP was 0.24, while that of neat HDPE was 0.13. Both values were lower than those of the blends, indicating quicker relaxation processes compared to the blends. The λ values for the blends with 75/25 and 25/75 PP/HDPE weight ratios were 12.9 and 7.70, respectively, distinctly higher than the λ value of 0.63 observed for the 50/50 blend. For the 75/25 and 25/75 blends, the presence of dispersed phases, whether PP or HDPE, restricted the mobility of polymer chains in the matrix phases, resulting in prolonged relaxation processes. Notably, the blend with the 75/25 PP/HDPE weight ratio exhibited much higher values than the blend with the 25/75 PP/HDPE weight ratio due to the nanometer scale dispersion of the HDPE domains. However, the 50/50 blend exhibited a co-continuous morphology with large

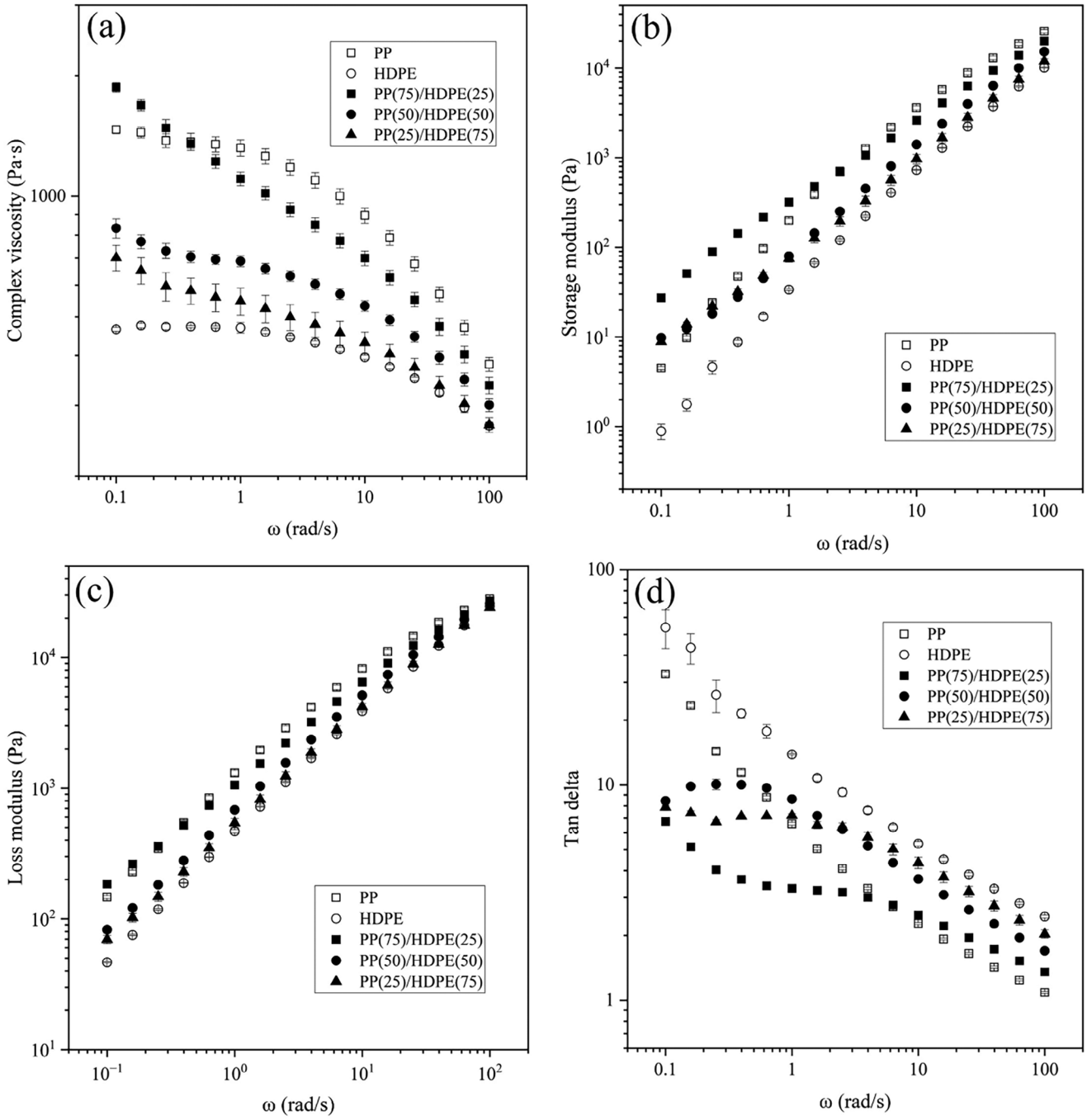

FIGURE 5 | Frequency sweeps of the PP, HDPE, and their blends: (a) complex viscosity, (b) storage modulus, (c) loss modulus, and (d) tan δ.

TABLE 1 | Zero-shear viscosity, characteristic times, and flow indexes fitted by the Cross Model.

Sample name	Zero-shear viscosity (η_0, Pa·s)	Characteristic time (λ, s)	Power-law index (n)	Coefficient of determination (R^2)
PP	1439	0.24	0.60	0.9953
PP(75)/HDPE(25)	2153	12.9	0.75	0.9883
PP(50)/HDPE(50)	781	0.63	0.79	0.9746
PP(25)/HDPE(75)	732	7.70	0.87	0.9731
HDPE	475	0.13	0.79	0.9972

PP and HDPE phase sizes, leading to less contact area compared to the sea-island morphologies. The results indicate that the λ values strongly correlated with the phase size and morphology.

The storage moduli of PP, HDPE, and their blends are plotted in Figure 5b. The storage modulus of PP was higher than that of HDPE throughout the testing frequency range. In the high frequency region, the storage modulus of the blend decreased with increasing HDPE content due to HDPE's greater flexibility compared to PP. Additionally, the storage modulus of the blend, regardless of the weight ratio, increased with frequency. This can be attributed to the high shear rates, which allowed less time for the polymer chains to relax, making the blends behave more rigidly. In the low frequency region, the storage modulus of the blend with the 75/25 PP/HDPE weight ratio is greater than that of PP. The presence of HDPE nanodomains enhanced deformation resistance by increasing interfacial friction between the PP and HDPE chains during flow, caused by viscosity differences, which increased the elastic response of the blend. The blends with 50/50 and 25/75 PP/HDPE weight ratios, when the frequency was lower than 0.2 rad/s, were also found to have greater storage moduli than neat PP due to similar reasons.

The loss moduli of PP, HDPE, and their blends are plotted in Figure 5c. In the high-frequency region, a similar trend was observed in the loss modulus as in the storage modulus. Both PP and HDPE, as well as their blends, tended to transition into glassy behavior under high shear rates, where polymer chains had insufficient time to respond to the applied stress. In the low frequency region, the blend with the 75/25 PP/HDPE weight ratio exhibited a higher loss modulus than neat PP at frequencies below 0.3 rad/s, as the presence of HDPE nanodomains altered the energy dissipation mechanism. Specifically, these nanodomains impeded the mobility of the PP chains, resulting in more energy being dissipated as heat to overcome the interfacial friction during chain movement.

The tangent of the phase angle (tan δ) value as a function of angular frequency is plotted in Figure 5d. Tan δ is a parameter used to understand material properties like damping, which is crucial for applications requiring efficient energy absorption and dissipation, such as automotive components and electronics packaging [58]. Both PP and HDPE, along with their blends, exhibited liquid-like behaviors at frequencies below 100 rad/s, as indicated by tan δ values >1. This suggests that the blends flow easily and are moldable, providing valuable insights for selecting processing conditions in manufacturing methods such as injection molding and extrusion. Lower tan δ values of the blends in the low frequency region, compared with those of PP and HDPE, confirmed the transition of the blend toward more elastic behavior due to constrained polymer chain mobility. The blend with the 75/25 PP/HDPE weight ratio exhibited the lowest tan δ value, indicating a more pronounced influence from uniformly dispersed HDPE nanodomains.

The Cole-Cole plots of PP, HDPE, and their blends are presented in Figure 6. The Maxwellian-like behaviors, indicated by a single semicircular arc, were observed on both PP and HDPE, indicating only one relaxation process [59]. The arc radius of PP was larger than that of HDPE because the PP used in this study demonstrated a longer relaxation time, as indicated by the result

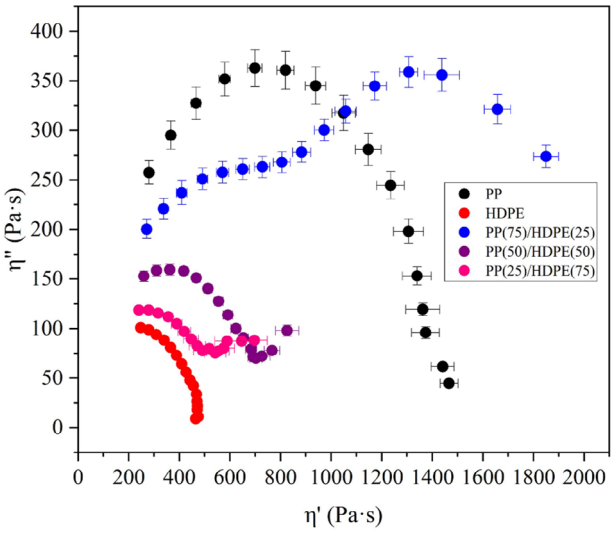

FIGURE 6 | Cole–Cole plots of PP, HDPE, and their blends.

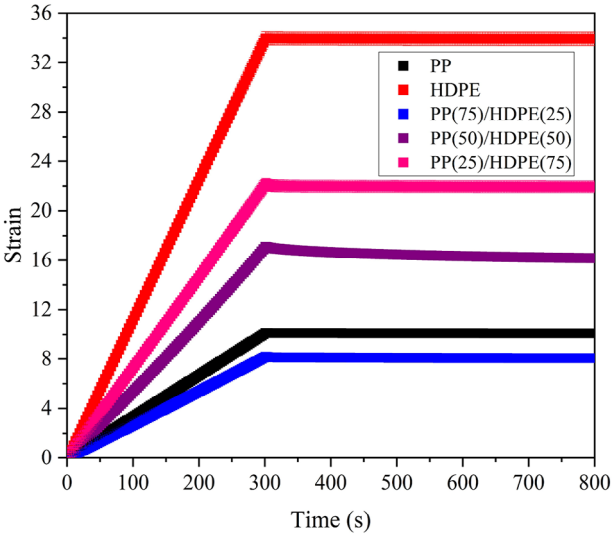

FIGURE 7 | Creep-recovery behaviors of PP, HDPE, and their blends.

fitted via Cross model. The blend with the 75/25 PP/HDPE weight ratio exhibited two arcs, reflecting two relaxation processes and implying the immiscibility of PP and HDPE components in the blend [60]. Compared to PP, two relaxation processes contributed to a longer total relaxation time in the 75/25 PP/HDPE ratio blend, indicating enhanced elastic behavior and greater resistance to flow due to the nanometer scale dispersion of HDPE domains. Two relaxation processes were also observed in the blends with 50/50 and 25/75 PP/HDPE ratios, although the shapes of the second arcs were not well-defined, indicating the immiscibility of PP and HDPE in these blends. The distortion in the shapes of the second arcs can be attributed to the less uniform domain sizes and distribution of the dispersed phases in these blends.

3.4.2 | Creep-Recovery Behaviors

The creep-recovery curves of PP, HDPE, and their blends are shown in Figure 7. During the creep stage, neat HDPE

TABLE 2 | Zero-shear viscosity calculated from creep tests.

Sample name	Zero-shear viscosity ($\eta_{0\text{-}C}$, Pa·s)
PP	1476 ± 19
PP(75)/HDPE(25)	1813 ± 10
PP(50)/HDPE(50)	856 ± 18
PP(25)/HDPE(75)	675 ± 14
HDPE	411 ± 8

showed lower resistance to creep deformation, as indicated by a greater change in strain over time compared to neat PP. As the PP content increased, the blends exhibited enhanced resistance to creep deformation. Specifically, the blend with the 75/25 PP/HDPE weight ratio demonstrated a smaller change in strain than the neat PP, suggesting improved elasticity. This enhancement is attributed to the uniform dispersion of HDPE nanodomains within the PP matrix, as explained in the frequency sweep results, which impeded chain mobility and increased the rigidity of the blend. During the recovery stage, PP and HDPE displayed near-ideal viscous behavior with almost no recovery, suggesting irreversible deformation. This is attributed to their more liquid-like behaviors under the high temperatures used in this study. However, slight recoveries were observed in the blends, as the presence of dispersed phases altered the chain entanglement within the matrix polymer, thereby enabling more elastic responses. Interestingly, the blend with the 50/50 PP/HDPE weight ratio showed a relatively higher proportion of recovery than the others, likely benefiting from the co-continuous morphology. This interpenetrated network potentially acted as a scaffold that more easily guided the polymer chains back toward their original and less oriented states after removing the stress.

The creep zero-shear viscosity ($\eta_{0\text{-}C}$, Pa·s) values were calculated from the steady-state flow range in creep tests, where the material exhibits purely viscous deformation at a constant rate [57], using Equation (3):

$$\eta_{0-C} = \frac{\sigma}{\dot{\gamma}} \tag{3}$$

where σ represents the constant stress applied to the material during the creep test, $\dot{\gamma}$ is the shear rate determined from the slope of the strain versus time curve in the steady-state flow range, and $\eta_{0\text{-}C}$ is the calculated creep zero-shear viscosity value. The $\eta_{0\text{-}C}$ values are shown in Table 2. The calculated $\eta_{0\text{-}C}$ values showed a consistent trend with those zero-shear viscosity data obtained from Cross model in Table 1, with the greatest value found in the blend with the 75/25 PP/HDPE weight ratio, attributed to the uniform dispersion of HDPE nanodomains within the PP matrix.

3.5 | Non-Isothermal Crystallization Kinetics

3.5.1 | Crystallization Behaviors

The crystallization curves of PP, HDPE, and their blends at cooling rates of 5, 10, and 15°C min^{-1} are shown in Figure 8. At the cooling rate of 5°C min^{-1}, the crystallization peak temperature of PP was 115.9°C, while that of HDPE was 117.8°C (Figure 8a). The crystallization peaks of PP and HDPE in their blends merged for all weight ratios, exhibiting crystallization peak temperatures similar to that of neat HDPE. This phenomenon can be explained by the heterogeneous nucleation effect of HDPE, which allowed PP to begin crystallizing at higher temperatures [61]. In detail, the presence of HDPE in the blends advanced PP crystallization by providing sites for heterogeneous nucleation at interfaces. The degree of supercooling required to reach the critical energy state needed for PP nucleation was reduced, namely, PP molecular chains started to crystallize more easily [62]. Similar results were found at cooling rates of 10 and 15°C min^{-1}. However, at greater cooling rates, fewer crystalline regions were formed because the molecular chains had less time to rearrange and crystallize, consequently resulting in observed reductions in the crystallization peak temperatures of PP, HDPE, and their blends [63, 64].

The melting curves are provided in Figure S5, and the calculated degrees of crystallinity for PP, HDPE, and each blend are presented in Table 3. As the cooling rate increased, the degrees of crystallinity for both PP and HDPE phases decreased, as observed in neat polymers and their blends. Faster cooling rates gave polymer chains less time to transition from a disordered, melted state to an ordered, crystalline state, and the rapid reduction in temperature prevented them from organizing into well-defined crystalline structures, resulting in lower degrees of crystallinity [65].

The degree of crystallinity for the PP phase decreased with increasing HDPE content, regardless of cooling rates, as the HDPE phase confined PP chain mobility and thus interfered with the PP crystal growth. This spatial confinement could lead to smaller or less perfect PP spherulites, especially for immiscible blends, where the interfacial boundaries caused by phase separation can extensively obstruct the growth of crystals. Similarly, the degree of crystallinity for the HDPE phase decreased with increasing PP content in the blends with the 75/25 and 50/50 PP/HDPE weight ratios.

However, for the blend with the 25/75 PP/HDPE weight ratio, the degrees of crystallinity for the HDPE phase remained nearly unchanged compared to neat HDPE across all cooling rates. This occurred because the HDPE chains near the PP domains were constrained by interfacial tension, forcing them to align in specific directions [66]. This alignment promoted the formation of more ordered structures in some regions, offsetting the reduction in degree of crystallinity caused by the chain movement restriction.

Moreover, the crystallization of the dispersed phases in the blends was also influenced by the presence of the major phases. In the 75/25 PP/HDPE blend, the crystallization of HDPE was inhabited by the major PP phase, as it isolated pathways for a significant portion of HDPE chains to migrate into crystalline regions, resulting in a reduced degree of crystallinity for the HDPE phase. Similarly, in the 25/75 PP/HDPE blend, the crystallinity of PP was significantly reduced due to the influence of the major HDPE phase.

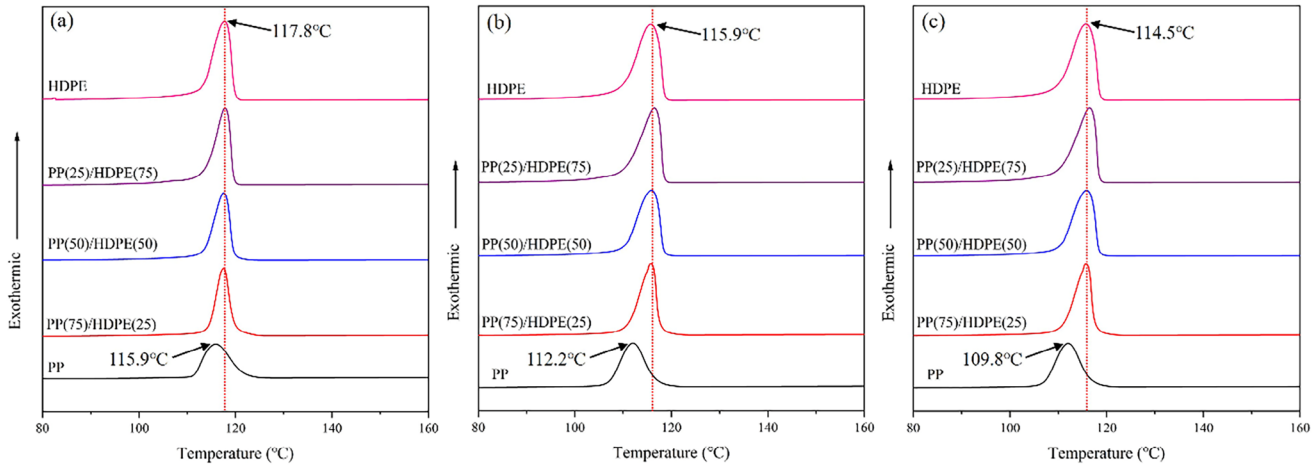

FIGURE 8 | Crystallization curves of PP, HDPE, and their blends at cooling rates of (a) 5°C min^{-1}, (b) 10°C min^{-1}, and (c) 15°C min^{-1}.

TABLE 3 | The degrees of crystallinity of PP, HDPE, and their blends at cooling rates of 5, 10, and 15°C min^{-1}.

Sample name	Degree of crystallinity [%]					
	5°C min^{-1}		10°C min^{-1}		15°C min^{-1}	
	PP	HDPE	PP	HDPE	PP	HDPE
PP	42.2 ± 0.7	–	40.5 ± 0.4	–	39.8 ± 0.4	–
PP(75)/HDPE(25)	41.3 ± 0.5	53.8 ± 0.4	39.3 ± 0.5	52.5 ± 0.8	38.8 ± 0.6	51.8 ± 0.7
PP(50)/HDPE(50)	37.2 ± 0.2	54.6 ± 0.4	37.1 ± 0.3	53.1 ± 0.5	36.5 ± 0.3	52.3 ± 0.6
PP(25)/HDPE(75)	33.4 ± 0.1	57.8 ± 0.2	33.3 ± 0.6	57.2 ± 0.2	32.8 ± 0.9	54.7 ± 0.4
HDPE	–	58.0 ± 0.3	–	57.1 ± 0.3	–	54.5 ± 0.4

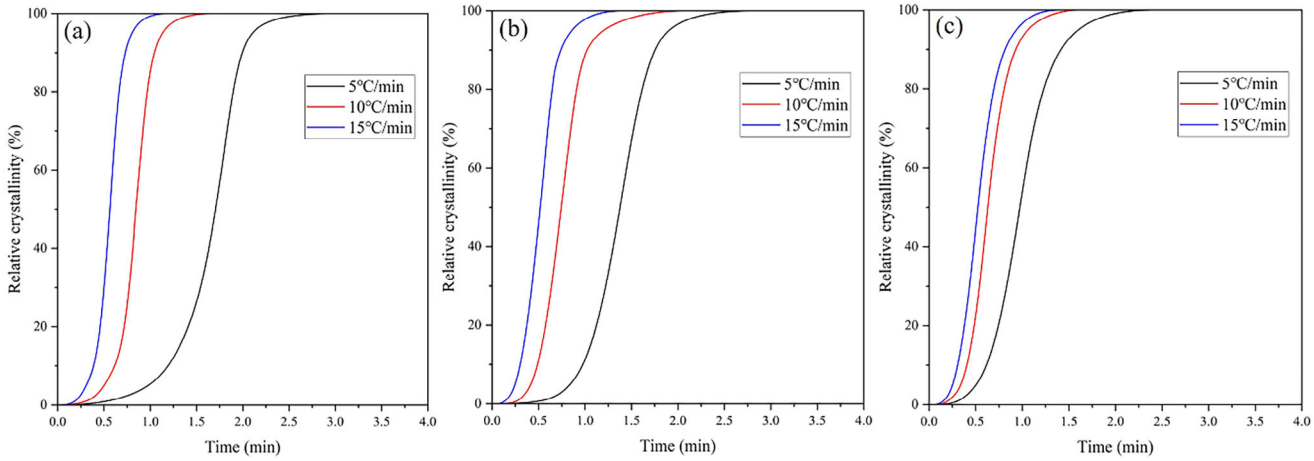

FIGURE 9 | Relative crystallinity as a function of crystallization time for the blends with different PP/HDPE weight ratios: (a) 75/25, (b) 50/50, and (c) 25/75. The relative crystallinity curves for neat PP and HDPE are provided in Figure S6.

3.5.2 | Relative Crystallinity

The evolutions of the relative crystallinity for blends as a function of crystallization time are presented in Figure 9 (The concept of relative crystallinity and the relevant equations are provided in Section S6.). All curves exhibited sigmoidal dependencies with increasing crystallization time, indicating that the crystallization was initially accelerated as the nuclei gradually formed and then slowed in later stages [67].

As the cooling rate increased, the crystallization was completed more quickly across all weight ratios due to greater degrees of

TABLE 4 | Fitted parameters by Avrami and Jeziorny models.

Sample name	Φ [°C min^{-1}]	Z_t	n	R^2	Zc	$t_{1/2}$ [min]
PP	5	0.14	2.94	0.9675	0.68	1.70
	10	0.84	3.05	0.9653	0.98	0.94
	15	1.68	3.11	0.9654	1.04	0.75
PP(75)/HDPE(25)	5	0.14	3.16	0.9465	0.68	1.65
	10	1.15	3.28	0.9586	1.01	0.86
	15	4.20	3.22	0.9753	1.10	0.57
PP(50)/HDPE(50)	5	0.20	3.41	0.9615	0.73	1.44
	10	1.16	3.28	0.9778	1.01	0.86
	15	4.08	3.03	0.9915	1.10	0.56
PP(25)/HDPE(75)	5	0.59	3.20	0.9913	0.90	1.05
	10	2.25	3.31	0.9930	1.08	0.70
	15	3.85	3.15	0.9944	1.09	0.56
HDPE	5	0.59	2.91	0.9923	0.90	1.06
	10	1.77	3.07	0.9933	1.06	0.74
	15	4.65	2.94	0.9951	1.11	0.52

undercooling, which occurred as the polymer melts were cooled below their crystallization temperatures more rapidly [42]. This enhanced undercooling significantly increased the nucleation rate by boosting the thermodynamic driving force necessary for forming crystalline nuclei, thereby leading to quicker formation of more nuclei and initiating the crystallization process more rapidly [68]. In detail, the change in thermodynamic driving force for the crystallization can be described by the change in Gibbs free energy (ΔG), given by Equation (4) [69]:

$$\Delta G = \Delta H - T\Delta S \tag{4}$$

where ΔH is the change in enthalpy of the system, T is the temperature at which the crystallization process occurs, and ΔS is the change in entropy of the system.

For the crystallization to occur spontaneously, ΔG must be negative [70]. Typically, during crystallization, ΔH is negative because the process is exothermic, and ΔS is negative as the system becomes more ordered, indicating a decrease in entropy. When the polymer melt was rapidly cooled at a higher cooling rate, a lower T value was achieved within a certain period, resulting in a less negative TΔS value. Consequently, the ΔG became a greater negative value, indicating a stronger thermodynamic driving force for crystallization. This increased driving force led to a higher nucleation rate, which accelerated the crystallization process.

3.5.3 | Avrami Model and Jeziorny Modification

The Avrami plots for blends with different weight ratios are shown in Figure S7, and the crystallization kinetic parameters derived from the Avrami plots and Jeziorny modification are listed in Table 4 (The concepts of the Avrami model and the Jeziorny modification, along with their relevant equations, are provided in Section S7.). The plots exhibited good linear relationships with most R^2 values around or above 0.97, indicating that the Avrami model can be used to describe the crystallization process of PP, HDPE, and their blends. This model was particularly reliable for the early stage of crystallization, as evidenced by the straighter lines compared to the more distorted shapes seen in later stage, aligning with other researchers' descriptions [71, 72].

The Z_c values increased with the cooling rate for all samples due to the greater undercooling achieved at higher cooling rates [42]. As mentioned earlier, this increased undercooling enhanced the thermodynamic driving force, compelling the system to crystallize more rapidly to minimize free energy [68]. Neat PP crystallized more slowly than neat HDPE, as indicated by the lower Z_c values, regardless of the cooling rate. Overall, compared to neat PP, increasing the HDPE content in the blends resulted in higher Zc values, attributed to heterogeneous nucleation driven by the PP and HDPE interfaces.

Notably, the blend with the 25/75 PP/HDPE weight ratio exhibited Zc values comparable to those of neat HDPE, despite containing 25 wt.% PP, which has an intrinsically lower crystallization rate than HDPE in this study. This can be explained by the presence of interfacial boundaries, which contributed to an increased crystallization rate. Specifically, as described earlier, the interfacial constraints experienced by HDPE chains near these boundaries helped align the chains and facilitated crystallization [66].

The n values for PP and HDPE were ≈3, indicating 3D spherulitic growth, a typical characteristic of semicrystalline polymers where crystals expand isotropically in all directions [73]. For blends, the average n values from different cooling rates were higher than those of PP and HDPE. This increase is likely due to enhanced nucleation driven by heterogeneous mechanisms at the interfaces, leading to complex crystallization behaviors.

TABLE 5 | Fitted parameters by Ozawa model.

Sample name	T [°C]	K(T)	m	R^2
PP	116	212	3.50	0.9998
	117	229	3.84	0.9990
	118	315	4.34	0.9992
PP(75)/HDPE(25)	116	234	3.00	0.9773
	117	334	3.65	0.9980
	118	296	4.10	0.9981
PP(50)/HDPE(50)	116	55.3	2.29	0.9724
	117	245	3.50	0.9324
	118	1840	5.25	0.9519
PP(25)/HDPE(75)	116	58.2	2.29	0.9238
	117	296	3.54	0.8844
	118	2981	5.47	0.9327
HDPE	116	21.2	1.81	0.9999
	117	43.4	2.55	0.9924
	118	612	4.60	0.9773

The crystallization half-time ($t_{1/2}$) refers to the time required to reach 50% relative crystallinity, serving as an indicator of the overall crystallization rate. A smaller $t_{1/2}$ value signifies a faster overall crystallization rate. This parameter can be determined using Equation (5) [74]:

$$t_{1/2} = \left(\frac{\ln 2}{Z_t}\right)^{1/n} \tag{5}$$

The $t_{1/2}$ values for PP, HDPE, and their blends were calculated and are included in Table 4. The $t_{1/2}$ value decreased with the increase in HDPE content in the blends, indicating a shortened crystallization time, which is consistent with the trend observed in Z_c values, confirming the increased crystallization rate.

3.5.4 | Ozawa Model

The Ozawa plots for the blends are provided in Figure S8, and the corresponding crystallization kinetic parameters derived from these plots are listed in Table 5 (The concept of the Ozawa model and the relevant equations are provided in Section S8.). The R^2 values for PP, HDPE, and their blend with the 75/25 PP/HDPE weight ratio were greater than 0.97, indicating good linear relationships. However, for blends with 50/50 and 25/75 PP/HDPE weight ratios, the deviations were evident, with low R^2 values, implying that the Ozawa model is inappropriate for describing the crystallization kinetics of these blends. This is likely due to the impact of phase morphology, where the coarser morphologies in the 50/50 and 25/75 ratio blends, compared to the uniform nanometer scale dispersion in the 75/25 ratio blend, resulted in uneven nucleation and chain growth, causing deviations in the Ozawa model's results.

In PP, HDPE, and their blend with the 75/25 PP/HDPE weight ratio, higher K(T) values were observed at higher temperatures, suggesting higher crystallization rates. Higher temperatures provided the polymer chains with more energy, facilitating nucleation and allowing the chains to reorganize into ordered structures more easily and rapidly. Similarly, higher m values were found at higher temperatures, reflecting the more pronounced influence of temperature on the crystallization kinetics. The K(T) values for PP were higher than those for HDPE at 116 and 117 °C, whereas at 118 °C, the K(T) value for PP was lower than that for HDPE. This is likely due to PP and HDPE being at different crystallization stages at these temperatures. PP crystallized more slowly and had a lower crystallization peak temperature than HDPE, regardless of the cooling rate, as shown in the crystallization half-time (Table 4) and crystallization peak temperature (Figure 8). At 116 and 117 °C, PP was still in a stage where abundant nuclei were forming, exhibiting a high crystallization rate, while HDPE had already transitioned to the next stage, where fewer nuclei were forming, and the crystallization rate was decreasing. However, at 118 °C, HDPE was at a stage where the crystallization rate was relatively high, resulting in a high K(T) value. For the blend with the 75/25 PP/HDPE weight ratio, higher K(T) values were obtained at 116 and 117 °C compared to PP, due to HDPE's heterogeneous nucleation. However, at 118 °C, the K(T) value of the blend was lower than that of PP, likely due to more complex crystallization kinetics associated with chain mobility influenced by nanometer-scale HDPE dispersion. This temperature-dependent complex crystallization kinetic could also explain why the Ozawa model is not well-suited for analyzing the crystallization kinetics of the binary blend of PP and HDPE, as both are semicrystalline polymers with different crystallization rates and temperatures.

3.5.5 | Mo Model

The Mo plots for blends are displayed in Figure S9, and the corresponding crystallization kinetic parameters derived from these plots are shown in Table 6 (The concept of the Mo model and the relevant equation are provided in Section S9.). The R^2 values were greater than 0.98 for PP, HDPE, and their blends, indicating that the Mo model effectively described their crystallization processes.

The F(T) values increased for all samples as the relative crystallinity increased, indicating a decreasing crystallization rate. This can be due to two major reasons: 1) a reduced number of polymer chains in the amorphous state and 2) limited regions available for nucleation and crystal growth. As crystallization proceeded, fewer polymer chains remained in the amorphous state for further transformation into crystalline structures. Meanwhile, existing crystals continued to grow and expand, reducing the available regions for new nucleation sites and physically obstructing crystal growth as they encountered each other.

With the increase in HDPE content, regardless of the relative crystallinity, the F(T) value decreased, ascribed to the heterogeneous nucleation effect at the interfaces. Interestingly, the blend with the 25/75 PP/HDPE weight ratio had even slightly lower F(T) values than neat HDPE. At this weight ratio, the presence of interfacial boundaries accelerated the crystallization of HDPE, as indicated by the results from the degree of crys-

TABLE 6 | Fitted parameters by the Mo model.

Sample name	X [%]	F(T)	α	R^2
PP	20	7.34	1.31	0.9901
	40	9.67	1.27	0.9898
	60	11.3	1.23	0.9893
	80	12.9	1.20	0.9883
PP(75)/HDPE(25)	20	7.08	0.98	0.9988
	40	8.12	0.98	0.9999
	60	8.85	1.00	0.9999
	80	9.72	1.05	0.9999
PP(50)/HDPE(50)	20	5.66	1.00	0.9992
	40	6.68	1.09	0.9999
	60	7.68	1.16	0.9999
	80	8.91	1.20	0.9999
PP(25)/HDPE(75)	20	3.08	1.64	0.9999
	40	4.18	1.71	0.9964
	60	5.30	1.78	0.9911
	80	7.22	1.87	0.9851
HDPE	20	3.26	1.54	0.9903
	40	4.56	1.59	0.9933
	60	5.91	1.57	0.9935
	80	7.55	1.58	0.9954

tallinity and the Avrami model, leading to a lower F(T) value. The inherent incompatibility between PP and HDPE potentially facilitated HDPE crystallization, as the high interfacial tension allowed for more favorable alignment and packing of HDPE polymer chains into crystalline structures. However, this also created a physical barrier that restricted the mobility of polymer chains, thereby hindering crystal growth. There was a complex competition between the initially favorable alignment and the subsequent physical barrier, with the dominant effect likely

TABLE 7 | The crystallization activation energy values of PP, HDPE, and their blends.

Sample name	Crystallization activation energy [ΔE, kJ mol^{-1}]	R^2
PP	−231	0.9990
PP(75)/HDPE(25)	−445	0.9866
PP(50)/HDPE(50)	−403	0.9840
PP(25)/HDPE(75)	−401	0.9365
HDPE	−435	0.9956

determined by the phase morphology. The micrometer scale dispersion morphology of PP in HDPE in the 25/75 PP/HDPE blend resulted in a less pronounced physical barrier compared to the nanometer scale dispersion morphology of HDPE in PP in the 75/25 PP/HDPE blend. This is because more boundaries formed at nanometer scale dispersion, which created more confined spaces due to physical constraints and hindered polymer chain mobility, preventing the chains from transferring to the growing crystal surface and inhibiting crystal growth [75].

The blends with 75/25 and 50/50 PP/HDPE weight ratios exhibited lower α values than those of neat PP and HDPE, while the blend with the 25/75 weight ratio displayed higher α values than both neat PP and HDPE, regardless of the degree of relative crystallinity. These observations are associated with both nucleation and restriction effects. For the blend with the 75/25 PP/HDPE weight ratio, the restriction on crystal growth was relatively pronounced because the nanometer scale dispersed HDPE phases resulted in a higher contact surface area, thereby lowering the α value. In the 50/50 weight ratio blend, which exhibited a co-continuous morphology, nucleation was less efficient compared to other blends where PP or HDPE phases were dispersed in smaller domains. Additionally, the existing boundaries between PP and HDPE phases continued to impact chain mobility and, consequently, crystal growth, leading to a reduction in the α value. Conversely, in the blend with the PP/HDPE 25/75 weight ratio, the restriction of chain mobility by phase boundaries contributed less to the overall effect than the heterogeneous nucleation, leading to a higher α value.

3.5.6 | Kissinger Model

The Kissinger plots for PP, HDPE, and their blends are shown in Figure S10, and the corresponding ΔE values obtained from these plots are listed in Table 7 (The concept of the Kissinger model and the relevant equation are provided in Section S10.). All R^2 values exceeded 0.98, except for the blend with the 25/75 PP/HDPE weight ratio, indicating strong linear relationships and affirming the reliability of Kissinger model in describing the crystallization process in this study.

The absolute value of ΔE ($|\Delta E|$) for HDPE was higher than that for PP, indicating that HDPE required more energy to overcome

the entropy barrier and align its chains into a crystalline state, which is consistent with the results found in Arshad's work [76]. This is associated with the higher degree of crystallinity in HDPE, as indicated in Table 3. More energy was needed for HDPE polymer chains to pack closely together, forming more extensive and perfect crystalline regions. For the blend with the 75/25 PP/HDPE weight ratio, a remarkable increase in |ΔE| value was observed by incorporating 25 wt.% HDPE, exceeding that of neat HDPE. This increase can be ascribed to the nanometer scale dispersion of HDPE domains within the PP matrix, which significantly restricted polymer chain mobility and consequently required more energy for crystal growth. For the blends with 50/50 and 25/75 PP/HDPE weight ratios, the calculated |ΔE| values were similarly greater than the theoretical |ΔE| values needed to overcome the energy barriers for initiating crystal growth of individual PP and HDPE in the corresponding amounts of the blends. However, the restriction effect on chain mobility was less pronounced because of the absence of nanometer scale phase morphology in these two blends.

4 | Conclusions

This work investigated mechanical properties, morphologies, rheology, and non-isothermal crystallization kinetics of PP, HDPE, and their blends with different weight ratios to elucidate the impact of phase morphology. Morphological observations revealed that at the 75/25 PP/HDPE weight ratio, HDPE phases were dispersed within the PP matrix on the nanometer scale, while at the 25/75 PP/HDPE weight ratio, PP phases were dispersed within the HDPE matrix on the micrometer scale. Additionally, a co-continuous morphology was formed at the 50/50 weight ratio. Mechanical testing revealed that co-continuous morphology was more effective at dissipating energy compared to matrix-dispersed morphology. FTIR spectroscopy results indicated that no chemical reactions occurred during the blend processing. Increases in complex viscosity, storage modulus, loss modulus, and creep resistance were observed in the low frequency region for the 75/25 weight ratio PP/HDPE blend due to the restriction effects of nanometer scale dispersed HDPE phases in the PP matrix. Meanwhile, significantly improved zero-shear viscosity was consistently observed for this nanometer scale dispersed morphology in both the Cross model predictions and creep tests. Similar but less pronounced phenomena appeared in other blends. Cole–Cole plots emphasized the immiscibility and twofold relaxation processes of the blends. DSC results showed elevated crystallization temperatures for the PP phases in the blends, attributed to HDPE's heterogeneous nucleation effect. Non-isothermal crystallization kinetic analyses employing different models consistently discovered that the crystallization rate of the blend increased with higher HDPE contents. Particularly, the blend with the 25/75 PP/HDPE weight ratio had a higher crystallization rate than neat HDPE, resulting from enhanced chain alignment promoted by interfacial boundaries. The dominant crystal growth geometry was 3D spherulitic growth, with blends exhibiting more complex crystallization kinetics than neat PP and HDPE. Nanometer scale dispersion in blends evidently restricted chain mobility during crystal growth, requiring higher crystallization activation energy.

This comprehensive study illustrated the profound impact of phase morphology on the properties of immiscible PP/HDPE blends. Future efforts will focus on tailoring these properties by manipulating the morphology of the dispersed phase using different compatibilization strategies.

Author Contributions

Ke Zhan: Conceptualization, data curation, formal analysis, investigation, methodology, writing – original draft. **Pixiang Wang:** Formal analysis, writing – review and editing. **Xueqi Wang:** Data curation, formal analysis. **Xiaomeng Li:** Data curation, formal analysis. **Shaoyang Liu:** Writing – review and editing. **Thomas Elder:** Writing – review and editing. **Brian Via:** Writing – review and editing. **Chuanbing Tang:** Writing – review and editing. **Yucheng Peng:** Conceptualization, funding acquisition, supervision, writing – review and editing.

Acknowledgements

This study was financially supported by the College of Forestry, Wildlife and Environment of Auburn University, the USDA National Institute of Food and Agriculture (McIntire Stennis project ALAZ00079), and the National Science Foundation (2132093). We acknowledge ExxonMobil Chemical Company for providing PP and HDPE pellets.

Conflicts of Interest

The authors declare no conflicts of interest.

Data Availability Statement

The data that support the findings of this study are available from the corresponding author upon reasonable request.

References

1. M. Chu, W. Tu, S. Yang, et al., "Sustainable Chemical Upcycling of Waste Polyolefins by Heterogeneous Catalysis," *SusMat* 2 (2022): 161.

2. Y. Miao, Y. Zhao, G. I. N. Waterhouse, R. Shi, L. Z. Wu, and T. Zhang, "Photothermal Recycling of Waste Polyolefin Plastics Into Liquid Fuels With High Selectivity Under Solvent-Free Conditions," *Nature Communications* 14 (2023): 4242.

3. X.-Y. Wang, Y. Gao, and Y. Tang, "Sustainable Developments in Polyolefin Chemistry: Progress, Challenges, and Outlook," *Progress in Polymer Science* 143 (2023): 101713.

4. W. Qu, Z. Bi, C. Zou, and C. Chen, "Light, Heat, and Force-Responsive Polyolefins," *Advanced Science* 11 (2024): 2307568.

5. R. S. Mohammadi, A. M. Zolali, J.-H. Kim, A. Jalali, and C. B. Park, "3D Fibrillated Network of Compatibilized Linear Low Density Polyethylene/Polyamide With High Melt Strength and Superior Foamability," *Polymer* 228 (2021): 123911.

6. X. Li, N. A. Mahadas, M. Zhang, J. DePodesta, M. Stefik, and C. Tang, "Sustainable High-Density Polyethylene via Chemical Recycling: From Modification to Polymerization Methods," *Polymer* 295 (2024): 126698.

7. M. Kheradmandkeysomi, A. Salehi, A. Jalali, H. Akrami, and C. B. Park, "Achieving Super-Tough High-Density Polyethylene With promising Foamability Using Silane Crosslinked Polyolefin Elastomer Nanofibrils Network," *Composites Science and Technology* 251 (2024): 110576.

8. E. Karaagac, T. Koch, and V. Archodoulaki, "Choosing an Effective Compatibilizer for a Virgin HDPE Rich-HDPE/PP Model Blend," *Polymers* 13 (2021): 3567.

9. T. Thiounn and R. C. Smith, "Advances and Approaches for Chemical Recycling of Plastic Waste," *Journal of Polymer Science* 58 (2020): 1347.

10. K. Jin, P. Vozka, C. Gentilcore, G. Kilaz, and N.-H. L. Wang, "Low-Pressure Hydrothermal Processing of Mixed Polyolefin Wastes Into Clean Fuels," *Fuel* 294 (2021): 120505.

11. J. Xu, J. M. Eagan, S.-S. Kim, et al., "Compatibilization of Isotactic Polypropylene (iPP) and High-Density Polyethylene (HDPE) With i PP–PE Multiblock Copolymers," *Macromolecules* 51 (2018): 8585.

12. M. Nofar, B. S. Yenigul, B. Ozdemir, C. Y. Kovanci, A. Ghanbari, and A. Jalali, "Mechanical and Viscoelastic Properties of Polyethylene-Based Microfibrillated Composites From 100% Recycled Resources," *Journal of Applied Polymer Science* 138 (2021): 50793.

13. D. Hassanian-Moghaddam, N. Asghari, and M. Ahmadi, "Circular Polyolefins: Advances Toward a Sustainable Future," *Macromolecules* 56 (2023): 5679.

14. K. Klimovica, S. Pan, T. W. Lin, et al., "Compatibilization of iPP/HDPE Blends with PE-g-iPP Graft Copolymers," *ACS Macro Letters* 9 (2020): 1161–1166.

15. J. Saleem, M. Z. Khalid Baig, U. B. Shahid, R. Luque, and G. McKay, "Mixed Plastics Waste Valorization to High-Added Value Products via Thermally Induced Phase Separation and Spin-Casting," *Green Energy & Environment* 9 (2024): 1627.

16. H. Jones, J. McClements, D. Ray, C. S. Hindle, M. Kalloudis, and V. Koutsos, "Thermomechanical Properties of Virgin and Recycled Polypropylene—High-Density Polyethylene Blends," *Polymers* 15 (2023): 4200.

17. C. Aumnate, N. Rudolph, and M. Sarmadi, "Recycling of Polypropylene/Polyethylene Blends: Effect of Chain Structure on the Crystallization Behaviors," *Polymers* 11 (2019): 1456.

18. M. Kheradmandkeysomi, A. Salehi, A. Jalali, et al., "Enhancing Mechanical Performance of High-Density Polyethylene at Different Environmental Conditions with Outstanding Foamability through In-Situ Rubber Nanofibrillation: Exploring the Impact of Interface Modification," *ACS Applied Materials & Interfaces* 16 (2024): 29291–29304.

19. K. M. E. Stewart, E. Stonecipher, H. Ning, and S. B. Pillay, "Mixing Rules for High Density Polyethylene-Polypropylene Blends," *The Canadian Journal of Chemical Engineering* 101 (2023): 5395.

20. M. Zhou, D. Mi, F. Hou, and J. Zhang, "Tailored Crystalline Structure and Mechanical Properties of Isotactic Polypropylene/High Molecular Weight Polyethylene Blend," *Industrial & Engineering Chemistry Research* 56 (2017): 8385.

21. J.-H. Lin, Y.-J. Pan, C.-F. Liu, et al., "Preparation and Compatibility Evaluation of Polypropylene/High Density Polyethylene Polyblends," *Materials* 8 (2015): 8850.

22. D. W. Bartlett, J. W. Barlow, and D. R. Paul, "Mechanical Properties of Blends Containing HDPE and PP," *Journal of Applied Polymer Science* 27 (1982): 2351.

23. F.-C. Chiu, H.-Z. Yen, and C.-E. Lee, "Characterization of PP/HDPE Blend-Based Nanocomposites Using Different Maleated Polyolefins as Compatibilizers," *Polymer Testing* 29 (2010): 397.

24. A. Verberckmoes, E. Fernandez, C. Martins, et al., "Morphological Analysis of Mechanically Recycled Blends of High Density Polyethylene and Polypropylene With Strong Difference in Melt Flow Index," *Polymer* 300 (2024): 126999.

25. A. Graziano, S. Jaffer, and M. Sain, "Review on Modification Strategies of Polyethylene/Polypropylene Immiscible Thermoplastic Polymer Blends for Enhancing Their Mechanical Behavior," *Journal of Elastomers & Plastics* 51 (2018): 291.

26. P. Wolff, A. Dickert, W. P. Kretschmer, and R. Kempe, "i PP/PE Multiblock Copolymers for Plastic Blend Recycling Synthesized by Coordinative Chain Transfer Polymerization," *Macromolecules* 55 (2022): 6435.

27. E. Carmeli, S. E. Fenni, M. R. Caputo, A. J. Müller, D. Tranchida, and D. Cavallo, "Surface Nucleation of Dispersed Polyethylene Droplets in Immiscible Blends Revealed by Polypropylene Matrix Self-Nucleation," *Macromolecules* 54 (2021): 9100.

28. D. E. Huang, A. P. Kotula, C. R. Snyder, and K. B. Migler, "Crystallization Kinetics in an Immiscible Polyolefin Blend," *Macromolecules* 55 (2022): 10921.

29. Y. Wang, H. Zou, Q. Fu, G. Zhang, K. Shen, and R. Thomann, "Shear-Induced Morphological Change in PP/LLDPE Blend," *Macromolecular Rapid Communications* 23 (2002): 749–752.

30. N. Vranjes and V. Rek, "Effect of EPDM on Morphology, Mechanical Properties, Crystallization Behavior and Viscoelastic Properties of iPP+HDPE Blends," *Macromolecular Symposia* 258 (2007): 90.

31. Z. O. G. Schyns and M. P. Shaver, "Mechanical Recycling of Packaging Plastics: A Review," *Macromolecular Rapid Communications* 42 (2021): 2000415.

32. A. Souza and N. Demarquette, "Influence of Composition on the Linear Viscoelastic Behavior and Morphology of PP/HDPE Blends," *Polymer* 43 (2002): 1313.

33. E. Karaagac, T. Koch, and V. M. Archodoulaki, "The Effect of PP Contamination in Recycled High-Density Polyethylene (rPE-HD) From Post-Consumer Bottle Waste and Their Compatibilization With Olefin Block Copolymer (OBC)," *Waste Management* 119 (2021): 285.

34. S. A. Ahmad Ramazani, M. Abdi Valami, and M. Khak, "Effect of Poly (Propylene-g-maleic Anhydride) on the Morphological, Rheological, and Mechanical Properties of PP/HDPE Blend," *Journal of Thermoplastic Composite Materials* 22 (2009): 519.

35. A. Al-Mulla and H. Shaban, "Study on Compatibility of Recycled Polypropylene/High-Density Polyethylene Blends Using Rheology," *Polymer Bulletin* 71 (2014): 2335.

36. H. Gao, Y.-m. Song, Q.-w. Wang, Z. Han, and M.-l. Zhang, "Rheological and Mechanical Properties of Wood Fiber-PP/PE Blend Composites," *Journal of Forestry Research* 19 (2008): 315.

37. A. K. Dhibar, J. K. Kim, and B. B. Khatua, "Cocontinuous Phase Morphology of Asymmetric Compositions of Polypropylene/High-Density Polyethylene Blend by the Addition of Clay," *Journal of Applied Polymer Science* 119 (2010): 3080.

38. R. Spina, M. Spekowius, and C. Hopmann, "Multi-Scale Thermal Simulation of Polymer Crystallization," *International Journal of Material Forming* 8 (2014): 497.

39. S. Jose, A. S. Aprem, B. Francis, et al., "Phase Morphology, Crystallisation Behaviour and Mechanical Properties of Isotactic Polypropylene/High Density Polyethylene Blends," *European Polymer Journal* 40 (2004): 2105.

40. R. Zhang, A. Jalali, K. Zhang, et al., "Tunable β-Crystals Formation From Transcrystallinity to Cylindrites at PP/PE Interface via Using Melt Penetration Engineering," *Polymer* 258 (2022): 125303.

41. P. K. Patra, A. Jaisingh, V. Goel, G. S. Kapur, and L. Nebhani, "Crystallization Kinetics of Compatibilized Blends of Polypropylene and Polyethylenimine," *Journal of Thermal Analysis and Calorimetry* 147 (2021): 6689.

42. M. Y. Ong and W. S. Chow, "Kinetics of Crystallization for Polypropylene/Polyethylene/Halloysite Nanotube Nanocomposites," *Journal of Thermoplastic Composite Materials* 33 (2018): 451.

43. H. P. Blom, J. W. Teh, T. Bremner, and A. Rudin, "Isothermal and Non-Isothermal Crystallization of PP: Effect of Annealing and of the Addition of HDPE," *Polymer* 39 (1998): 4011.

44. Y. Kong and J. N. Hay, "The Measurement of the Crystallinity of Polymers by DSC," *Polymer* 43 (2002): 3873.

45. J. A. Rodríguez-Liébana, M. A. Martín-Lara, F. J. Navas-Martos, et al., "Morpho-Structural and Thermo-Mechanical Characterization of Recycled Polypropylene and Polystyrene From Mixed Post-Consumer Plastic Waste," *Journal of Environmental Chemical Engineering* 10 (2022): 108332.

46. C. Spicker, N. Rudolph, I. Kühnert, and C. Aumnate, "The Use of Rheological Behavior to Monitor the Processing and Service Life Properties of Recycled Polypropylene," *Food Packaging and Shelf Life* 19 (2019): 174.

47. J. R. Barone, "Polyethylene/Keratin Fiber Composites With Varying Polyethylene Crystallinity," *Composites Part A: Applied Science and Manufacturing* 36 (2005): 1518.

48. C. Sibele Piedade and M. Luis Claudio, "Thermal Properties and Morphology of High-Density Polyethylene Filled With Coffee Dregs," *Journal of Thermal Analysis and Calorimetry* 114 (2013): 1.

49. C. Rosales, N. Aranburu, I. Otaegi, et al., "Improving the Mechanical Performance of LDPE/PP Blends Through Microfibrillation," *ACS Applied Polymer Materials* 4 (2022): 3369.

50. A. M. Zolali and B. D. Favis, "Compatibilization and Toughening of Co-Continuous Ternary Blends via Partially Wet Droplets at the Interface," *Polymer* 114 (2017): 277.

51. M. Maroufkhani, A. Katbab, H. Bizhani, and J. Zhang, "Toward Morphology Development and Impact Strength of Co-Continuous Supertough Dynamically Vulcanized Rubber Toughened PLA Blends: Effect of Sulfur Content," *Polymer* 217 (2021): 123439.

52. L. Wang, J. Lau, E. L. Thomas, and M. C. Boyce, "Co-Continuous Composite Materials for Stiffness, Strength, and Energy Dissipation," *Advanced Materials* 23 (2011): 1524.

53. N. D. Polychronopoulos and J. Vlachopoulos, "Polymer Processing and Rheology," in *Cellulose-Based Superabsorbent Hydrogels* (Springer, 2019): 1–27.

54. Y. Wang, W. Sun, S. Liu, et al., "The Formation of a Highly Oriented Structure and Improvement of Properties in PP/PA6 Polymer Blends During Extrusion-Stretching," *Polymers* 12 (2020): 878.

55. K. Zhan, D. Meadows, L. Levy, et al., "Impact of Thermomechanical Reprocessing on Multilayer Plastic Packaging Blend," *Polymer Degradation and Stability* 222 (2024): 110710.

56. P. Agrawal, M. H. A. Silva, S. N. Cavalcanti, et al., "Rheological Properties of High-Density Polyethylene/Linear Low-Density Polyethylene and High-Density Polyethylene/Low-Density Polyethylene Blends," *Polymer Bulletin* 79 (2021): 2321.

57. T. Mezger, *The Rheology Handbook*, (Vincentz Network, 2020).

58. A. Treviso, B. Van Genechten, D. Mundo, and M. Tournour, "Damping in Composite Materials: Properties and Models," *Composites Part B: Engineering* 78 (2015): 144.

59. D. J. Bischoff, T. Lee, K. S. Kang, et al., "Unraveling the Rheology of Inverse Vulcanized Polymers," *Nature Communications* 14 (2023): 7553.

60. P. Agrawal, A. P. M. Araújo, J. C. C. Lima, et al., "Rheology, Mechanical Properties and Morphology of Poly(lactic acid)/Ethylene Vinyl Acetate Blends," *Journal of Polymers and the Environment* 27 (2019): 1439.

61. S. E. Fenni, A. J. Müller, and D. Cavallo, "Understanding Polymer Nucleation by Studying Droplets Crystallization in Immiscible Polymer Blends," *Polymer* 264 (2023): 125514.

62. I. Shamseddine, F. Pennec, P. Biwole, and F. Fardoun, "Supercooling of Phase Change Materials: A Review," *Renewable and Sustainable Energy Reviews* 158 (2022): 112172.

63. S. Song, J. Jiang, E. Nikbin, J. Y. Howe, I. Manners, and M. A. Winnik, "The Role of Cooling Rate in Crystallization-Driven Block Copolymer Self-Assembly," *Chemical Science* 13 (2022): 396.

64. H. Tian, S. Zhang, X. Ge, and A. Xiang, "Crystallization Behaviors and Mechanical Properties of Carbon Fiber-Reinforced Polypropylene Composites," *Journal of Thermal Analysis and Calorimetry* 128 (2016): 1495.

65. S. Park, W. Shou, L. Makatura, W. Matusik, and K. Fu, "3D Printing of Polymer Composites: Materials, Processes, and Applications," *Matter* 2022, 5, 43.

66. N. Q. Nguyen, T.-F. Chen, and C.-T. Lo, "Confined Crystallization and Chain Conformational Change in Electrospun Poly(Ethylene Oxide) Nanofibers," *Polymer Journal* 53 (2021): 895.

67. Z.-f. Bai and Q. Dou, "Non-Isothermal Crystallization Kinetics of Polypropylene/Poly(Lactic Acid)/Maleic Anhydride-Grafted Polypropylene Blends," *Journal of Thermal Analysis and Calorimetry* 126 (2016): 785.

68. B. Crist and J. M. Schultz, "Polymer Spherulites: A Critical Review," *Progress in Polymer Science* 56 (2016): 1.

69. J. E. K. Schawe, "The Gibbs Free Energy Difference Between a Supercooled Melt and the Crystalline Phase Of Polymers," *Journal of Thermal Analysis and Calorimetry* 120 (2015): 1417.

70. P. U. Dhanvijay and V. V. Shertukde, "Review: Crystallization of Biodegradable Polymers," *Polymer-Plastics Technology and Engineering* 50 (2011): 1289.

71. K. Shirzad and C. Viney, "A Critical Review on Applications of the Avrami Equation Beyond Materials Science," *Journal of The Royal Society Interface* 20 (2023): 20230242.

72. F. C. Pérez-Ćardenas, L. F. D. Castillo, and R. Vera-Graziano, "Modified Avrami Expression for Polymer Crystallization Kinetics," *Journal of Applied Polymer Science* 43 (1991): 779.

73. A. Bénard and S. G. Advani, "A Cell Model to Describe the Spherulitic Growth in Semicrystalline Polymers," *Polymer Engineering & Science* 36 (1996): 520–534.

74. Y.-f. Zhang, H. Chen, B.-b. Liu, Y.-h. Gu, and X.-x. Li, "Isothermal and Non-Isothermal Crystallization of Isotactic Polypropylene Nucleated With 1,3,5-Benzenetricarboxylic Acid Tris(Cyclohexylamide)," *Thermochimica Acta* 590 (2014): 226.

75. Y. Zhang, B. Li, J. Liu, et al., "Inhibition of Crystal Nucleation and Growth: A Review," *Crystal Growth & Design* 24 (2024): 2645–2665.

76. A. M. Azeem, "Kinetics of Crystallization Mechanisms in High Density Polyethylene and Isotactic Polypropylene," *Polymer Science, Series A* 63 (2022): S23–S33.

Supporting Information

Additional supporting information can be found online in the Supporting Information section.

Supporting file 1: macp70043-sup-0001-SuppMat.docx